Potential Fields Generated by Oblique Dipole Layers Modeling Excitation Wavefronts in the Anisotropic Myocardium

Comparison with Potential Fields Elicited by Paced Dog Hearts in a Volume Conductor

Piero Colli-Franzone, Luciano Guerri, Carla Viganotti, Emilio Macchi, Silvana Baruffi, Santa Spaggiari, and Bruno Taccardi

From the Institute of Numerical Analysis, CNR, Pavia, Italy, the Institute for the Application of Calculus, CNR, Rome, Italy and the Institute of General Physiology, University of Parma, Italy

SUMMARY. The potential distribution in a homogeneous, cylindrical volume conductor surrounding an isolated paced dog heart was first measured and then calculated by using a mathematical model that simulates an anisotropic excitation wavefront spreading through the heart muscle. The study was performed with a view to establish to what extent the anisotropy of cardiac generators affects the potential field in the extra-cardiac conducting media at a great distance from the heart. The model considers an oblique dipole layer on the wavefront which, assuming axial symmetry of the electrical properties of the fibers, can be viewed as the superposition of an axial and a transverse dipole layer. These layers are, respectively, parallel and perpendicular to the local fiber direction. A notable feature of the model is that, in the case of axial symmetry, the potential field due to such an oblique distribution is also equivalent to the sum of the potentials generated, respectively, by a normal and an axial dipole layer. In this form, the model generalizes the classical, uniform double layer model, upon which the solid angle theory is based, by adding to it an axial component. The features of the measured potential fields, which could not be interpreted on the basis of the solid angle theory, were satisfactorily reproduced by the model, at least on a qualitative basis. The results clearly showed the dominant role played by the axial component of the potential field even at a considerable distance from the heart. (***Circ Res 51: 330-346, 1982***)

IN RECENT years, the theory which assumes a uniform dipole layer as a suitable equivalent generator of the extracellular potential field, elicited by a depolarization wavefront spreading in the myocardium, has been challenged by experimental evidence collected on the animal.

In 1977, Corbin and Scher showed that a current flow spreading from the front toward the resting tissue, as predicted by the uniform dipole layer model, occurred only where the excitation wavefront was moving along the main direction of myocardial fibers. Those parts of the wavefront that moved across fibers apparently did not generate currents flowing toward the resting tissue but received currents flowing from the resting tissue toward the wavefront.

The investigations by Baruffi et al. (1978) and Spaggiari et al. (1980), carried out under different experimental conditions, confirmed Corbin and Scher's views on the influence of cardiac fiber orientation on extracellular potentials. Two apparently different models of the bioelectric sources then were proposed with a view to reproducing adequately the potential distributions observed in these experiments. Corbin and Scher (1977) proposed the so-called axial model, consisting of current dipoles parallel to the local fiber direction. Spach et al. (1972, 1979) proposed a model of intracellular currents in which it was assumed that the shape of the action potential was the same in all cardiac cells and, by taking into account the anisotropy of intracellular conductivity, the equivalent bioelectric sources were defined in terms of transmembrane current distribution.

Both models imply a non-uniform current density distribution. However, the axial model does not specify whether the non-uniformity is due to *the anisotropy of the cardiac sources* or to the anisotropic conductivity, while in the model proposed by Spach et al., the non uniformity is derived from intracellular anisotropic conductivity.

We propose here a mathematical model which, given the geometry of the front and fibers, assumes an oblique dipole distribution on the front, related to the fiber direction. The aim of the model is to provide a description of the potential field at a distance from the sources, in a conducting medium surrounding the excitable tissue. In the following, we shall consider dipole distributions (or double layers) where the dipole direction is not necessarily perpendicular to the wavefront surface. This kind of double layer will be called "oblique double layer." To distinguish different cases, we shall talk of a "normal" dipole distribution when the dipole direction is perpendicular to

the front; of "axial" or "transverse" dipole distributions when the dipoles are parallel or perpendicular to the local fiber direction, respectively.

The model we propose generalizes Corbin and Scher's axial model in that it takes also into account the presence of dipoles oriented in a direction perpendicular to the fibers.

It will be shown that our model establishes a connection between Corbin and Scher's generalized model and a limit case of the model proposed by Spach et al., namely, when the upstroke of the action potential approaches a step function. Hence an oblique double layer model representing the bioelectric sources may also be obtained by assuming a constant jump of the intracellular action potential associated with an anisotropic intracellular conductivity.

A salient feature of the potential field generated by an oblique double layer in a homogeneous isotropic unbounded (or bounded) conducting medium is that the field may be seen as the superposition of the potential due to a normal and an axial dipole layer. For this reason, an oblique double layer model is an extension of the classical uniform and normal dipole layer model, obtained by adding to it an axial perturbation that makes the potential field dependent on the shape of the front and the orientation of the fibers.

Considering the potential field as the result of the combination of a normal and an axial component can be useful for a qualitative prediction of the general features of the field, once the geometry of the wavefront and the fiber direction are assigned.

The potential field generated by a wavefront in a homogeneous isotropic and bounded conducting medium was computed numerically by solving an integral boundary equation using the finite element method with collocation. Model simulations were performed to reproduce the data collected in isolated dog heart experiments after endocardial and intramural stimulations.

Finally, the influence of the model parameters on the matching between computed and measured potential patterns was investigated.

Methods

Electrical Measurements

Experiments were performed on six mongrel dogs weighing 20–25 kg. Each dog was anesthetized with iv pentobarbital-Na (30 mg/kg). The hearts were isolated and perfused according to Langendorff's method with blood from the carotid artery of a donor dog (Taccardi et al., 1972). Blood flowing from the pulmonary artery of the isolated heart was sent to the external jugular vein of the donor.

The isolated dog hearts were placed in the middle of a cylindrical tank, 15 cm high and 23 cm across, filled with a simplified Ringer's solution containing NaCl, 157 mM; KCl, 5.6 mM. $CaCl_2$ was not added, to prevent the forming of clots in the bath, due to the unavoidable slight leakage of blood from the preparation. The resistivity of the solution was about 50 Ohm cm.

An intramural multiterminal needle electrode was inserted into the left ventricular wall. The needle was provided with 10–15 Ag-AgCl terminals, 1 mm apart, 0.1 mm in diameter. Terminal 1 was located at the epicardial level.

Twelve comb-shaped electrode supports were placed in the bath at 15 degrees from one another, facing the left ventricular wall. Thus, approximately one half of the cylindrical conducting medium was explored by the electrode array. Each comb had 50 terminals fixed on horizontal steel rods covered with insulating material. On each rod the terminals were spaced 0.5 to 3.5 cm from one another (Fig. 1). The rods were arranged to slide radially so that their tips could be brought within 3–5 mm of the heart surface. The total number of lead points in the bath was 600.

Electrocardiograms were recorded from all the lead points in the conducting medium and on the intramural needle.

A common reference electrode was fixed close to the tank wall. At the end of each experiment the (cylindrical) coordinates of the terminals on the rods and needle were determined. The hearts were paced at the endocardial level or in the middle of the wall through couples of successive terminals on the needle. Stimuli of about 1.5 threshold level and 0.5 msec in duration were delivered at a frequency just above the spontaneous heart rate through a stimulus isolation unit.

One hundred terminals in the bath and all the terminals on the needle electrode were connected simultaneously to the input of a multi-channel instrument that performed on line amplification, multiplexing and digital conversion of the signals at the rate of one conversion per channel per msec (Cottini et al., 1972). The digital data were conveyed to a computer system. Successive sets of 100 terminals were sequentially connected to the instrument until all the 600 points had been explored. The terminals on the needle were permanently connected and the corresponding signals were used for time alignment.

The digital data were sent to a buffer memory that could trap 120 K bytes of information, corresponding to 1 second of recording. The output of the buffer memory was fed into a computer system (PDP 11/40) and stored on disk. The data were displayed on a video unit for quality control. When the signal-to-noise ratio was too low, the data were averaged on line by using a special routine of the microprocessor governing the buffer memory.

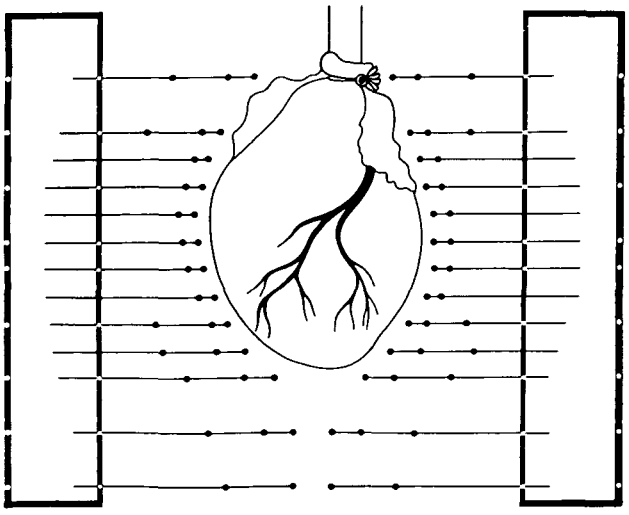

FIGURE 1. *Diagrammatic drawing illustrating the isolated dog heart in the cylindrical conducting medium. Two "combs" are shown, each of which supports 50 terminals. The terminals are indicated by block dots (on sliding rods) or white circles (on fixed vertical supports).*

The potential values then were printed on tables and the instantaneous distribution of equipotential lines was plotted on a series of horizontal planes and on ideal surfaces surrounding the heart at various distances in the conducting medium.

Mathematical Model

Oblique Dipole Layers in a Homogeneous Isotropic Medium

We shall here present a mathematical model of a depolarization wavefront suitable for a quantitative description of the potential field generated at distance from the cardiac sources. A way to formulate the model is to start from Corbin and Scher's axial model and to take into account also a dipole distribution on the wavefront oriented in a direction perpendicular to that of the fibers. We assume that the activating myocardial layer, comprised between the resting and the depolarized tissue, is so thin that the depolarization wavefront spreading through the myocardium, at time t, may be idealized as a moving surface $S = S(t)$. This assumption is best suited for describing the potential at some distance from the cardiac sources, e.g., outside the myocardium.

Let $\bar{n}$ be the unit vector normal to S and oriented in the direction of the advancing front, i.e., toward the resting tissue. Consequently, the region ahead and behind the front corresponds, respectively to the resting and to the depolarized heart tissue. Since the model was conceived for simulating the potential field at a distance from the sources, we shall consider the front S as imbedded into an unbounded, homogeneous, and isotropic medium with conductivity σ_0, thus neglecting the influence of the boundary between the intra- and extracardiac tissue as well as the anisotropy of the extracellular cardiac medium. This is a strong simplification because the real wavefront spreads through anisotropic, non-homogeneous heart tissue. However, in simulating the potential field measured at a distance from the sources in a homogeneous isotropic medium, we may expect the above simplification to affect the numerical values of the potential, but not the overall potential pattern. In order to simulate the potential field inside the myocardium, one should take into account the anisotropy of the myocardial tissue. Since the direction of myocardial fibers is not uniform, a still manageable model can be set up for a small portion of tissue, where the fibers can be assumed to be parallel. Such a model, which we call "local," has been developed in the Appendix. A similar local model has been independently developed by Roberts and Scher (1982), who used it to compute the potential near the wavefront.

For any point $\bar{y}$ on S, let $\bar{a}_\ell$ denote the unit vector parallel to the local fiber direction and pointing toward the resting tissue; hence it is $\bar{n}\cdot\bar{a}_\ell \geq 0$ (as usual, $\bar{a}\cdot\bar{b}$ denotes the scalar product of the vectors $\bar{a}$ and $\bar{b}$).

In the axial model, the equivalent source generators are represented by a dipole layer $\mu_\ell\bar{a}_\ell$ with density μ_ℓ (on S) given by $m_\ell(\bar{n}\cdot\bar{a}_\ell)$ with $m_\ell > 0$. In an unbounded homogeneous and isotropic medium with constant conductivity σ_0, this layer generates the potential:

$$U(\bar{x}) = \frac{1}{4\pi\sigma_0}\int_S u_\ell\bar{a}_\ell\cdot\nabla r^{-1}\,dS = \frac{1}{4\pi\sigma_0}\int_S m_\ell(\bar{n}\cdot\bar{a}_\ell)\bar{a}_\ell\cdot\nabla r^{-1}\,dS \quad (1)$$

where $\bar{r} = \bar{x} - \bar{y}$, $r = (\bar{r}\cdot\bar{r})^{1/2}$ and ∇ is the gradient vector operator with components $\partial/\partial x_1$, $\partial/\partial x_2$, $\partial/\partial x_3$ in a cartesian system of coordinates. Given $\bar{x}$, the integral is performed with respect to the $\bar{y}$ variable on S. It is $\mu_\ell = 0$ where the front is tangent to the fibers and $\mu_\ell = m_\ell$ (maximum value) where the front is perpendicular to the fibers. Since $dS_\ell = (\bar{n}\cdot\bar{a}_\ell)\,dS$ is the projection of the surface element dS on the plane perpendicular to $\bar{a}_\ell$, it follows that the contribution of the dipole $m_\ell\bar{a}_\ell$ located on dS is proportional to dS_ℓ. We shall call the layer $\mu_\ell\bar{a}_\ell$ and the potential $U(\bar{x})$ defined by Equation 1 the axial dipole layer and the axial potential, respectively.

We shall now extend the axial model, defined by Equation 1, by including generators in a direction transverse to that of the fibers. We shall make the following assumptions:

1. The fibers are axisymmetric with respect to the bioelectric properties in the sense that cardiac current sources act identically in any direction perpendicular to that of the fiber, i.e., if a locally parallel cell packing of fibers is considered, the occurrence of branching and lateral intercellular junctions are assumed to show identical frequency. This seems a reasonable assumption for a macroscopic model where the various kind of tissues are conceived as continuous media.

2. At any point of the wavefront, the equivalent source generators are characterized by an axial and a transverse dipole $m_\ell\bar{a}_\ell$, $m_t\bar{a}_t$. It is m_ℓ, $m_t \geq 0$; the unit vector $\bar{a}_t$ is perpendicular to $\bar{a}_\ell$ and, because of the axisymmetry of the fibers, the vectors $\bar{n}$, $\bar{a}_\ell$, $\bar{a}_t$ are coplanar. Moreover $\bar{a}_\ell$, $\bar{a}_t$ are oriented toward the resting tissue, so that $\bar{n}\cdot\bar{a}_\ell \geq 0$, $\bar{n}\cdot\bar{a}_t \geq 0$.

3. The dipole $m_t\bar{a}_t$ behaves in a manner similar to $m_\ell\bar{a}_\ell$ so that on S we have the transverse dipole layer $\mu_t\bar{a}_t$ with density $\mu_t = m_t(\bar{n}\cdot\bar{a}_t)$. This layer generates the transverse potential:

$$U(\bar{x}) = \frac{1}{4\pi\sigma_0}\int_S \mu_t\bar{a}_t\cdot\nabla r^{-1}\,dS = \frac{1}{4\pi\sigma_0}\int_S m_t(\bar{n}\cdot\bar{a}_t)\bar{a}_t\cdot\nabla r^{-1}\,dS \quad (2)$$

The potential due to both the axial and transverse dipole layers $\mu_\ell\bar{a}_\ell$, $\mu_t\bar{a}_t$ is given by the superposition of the corresponding potentials, i.e., by:

$$U(\bar{x}) = \frac{1}{4\pi\sigma_0}\int_S (\mu_\ell\bar{a}_\ell + \mu_t\bar{a}_t)\cdot\nabla r^{-1}\,dS = \frac{1}{4\pi\sigma_0}\int_S [m_\ell(\bar{n}\cdot\bar{a}_\ell)\bar{a}_\ell + m_t(\bar{n}\cdot\bar{a}_t)\bar{a}_t]\cdot\nabla r^{-1}\,dS \quad (3)$$

We remark that $\bar{n}$, $\bar{a}_\ell$, $\bar{a}_t$, m_ℓ, m_t depend on the point $\bar{y}$ varying on the front S, whereas r depends both on $\bar{x}$ and $\bar{y}$; therefore, since under the integral sign only r depends on $\bar{x}$, it follows that the potential $U(\bar{x})$ is harmonic.

In the model defined by Equation 3, m_ℓ and m_t need not be constant, If $m_t \equiv 0$ and m_ℓ is constant, we obtain Corbin and Scher's axial model.

Setting $\bar{b} = \mu_\ell\bar{a}_\ell + \mu_t\bar{a}_t$ and $\mu = (\bar{b}\cdot\bar{b})^{1/2}$, $\bar{a} = \bar{b}/\mu$, Equation 3 becomes:

$$U(\bar{x}) = \frac{1}{4\pi\sigma_0}\int_S \mu\bar{a}\cdot\nabla r^{-1}\,dS. \quad (4)$$

Note that, in Equation 4, the term $\mu\bar{a}$ coincides with $\mu_\ell\bar{a}_\ell$ or with $\mu_t\bar{a}_t$ if $m_t = 0$ (axial model) or $m_\ell = 0$ (transverse

model), that the dipole axis $\bar{a}$ is, in general, oblique to S, and that, when $m_\ell = m_t = m$, it results $\mu\bar{a} = m\bar{n}$ (normal model). Due to the fact that $\bar{a}$ is generally oblique to S, we shall name the dipole layer $\mu\bar{a}$, appearing in Equation 4, an oblique dipole layer (oblique model).

In treating dipole layers, it is customary to consider the density relative to the surface on which the dipoles are distributed. In tensor terms, it would be more natural to characterize the layer by means of the dipole moment tensor. In particular, with reference to the principle axes $\bar{a}_\ell$ and $\bar{a}_t$, we could consider the layers $m_\ell\bar{a}_\ell$ and $m_t\bar{a}_t$. The dipole moments m_ℓ and m_t represent directly a property of the equivalent source generators, whereas μ_ℓ and μ_t are dependent also on the normal $\bar{n}$ to the front. In this paper we make a limited use of tensor calculus and, for this reason, we shall use the notation $\mu_\ell\bar{a}_\ell$ and $\mu_t\bar{a}_t$ for the axial and the transverse dipole layers, respectively. From an oblique dipole layer, a normal layer is recovered under each of the following conditions:

When the front is tangent to the fibers, it is $\bar{n}\cdot\bar{a}_\ell = 0$ and $\bar{a}_t = \bar{n}$; in this case Equation 3 reduces to:

$$U(\bar{x}) = \frac{1}{4\pi\sigma_0}\int_S m_t\bar{n}\cdot\nabla r^{-1}\,dS \tag{5}$$

i.e., the potential is due to a normal dipole layer of density m_t.

When the front is perpendicular to the fibers, it is $\bar{n}\cdot\bar{a}_t = 0$ and $\bar{a}_\ell = \bar{n}$; in this case Equation 3 reduces to:

$$U(\bar{x}) = \frac{1}{4\pi\sigma_0}\int_S m_\ell\bar{n}\cdot\nabla r^{-1}\,dS \tag{6}$$

i.e., the potential is due to a normal dipole layer of density m_ℓ. Hence, one or the other of the two normal layers becomes dominant as the front tends to be tangent or perpendicular to the fibers.

A Useful Spit

We shall now show that the potential generated by the superposition of the transverse and axial dipole layers $\mu_t\bar{a}_t$ and $\mu_\ell\bar{a}_\ell$ according to Equation 3 can also be obtained by means of the normal dipole layer $m_t\bar{n}$ and the axial dipole layer $\mu_{\ell t}\bar{a}_\ell$ where $\mu_{\ell t} = (m_\ell - m_t)(\bar{n}\cdot\bar{a}_\ell)$. This result can be established in the following way. Since $\bar{n}$, $\bar{a}_\ell$, $\bar{a}_t$ are coplanar and $\bar{a}_\ell$, $\bar{a}_t$ are perpendicular, it follows that:

$$(\bar{n}\cdot\bar{a}_\ell)\bar{a}_\ell + (\bar{n}\cdot\bar{a}_t)a_t = \bar{n}.$$

Hence:

$$\begin{aligned} &m_t(\bar{n}\cdot\bar{a}_t)\bar{a}_t + m_\ell(\bar{n}\cdot\bar{a}_\ell)\bar{a}_\ell \\ &= m_t[(\bar{n}\cdot\bar{a}_t)\bar{a}_t + (\bar{n}\cdot\bar{a}_\ell)\bar{a}_\ell] \\ &\quad + (m_\ell - m_t)(\bar{n}\cdot\bar{a}_\ell)\bar{a}_\ell \\ &= m_t\bar{n} + (m_\ell - m_t)(\bar{n}\cdot\bar{a}_\ell)\bar{a}_\ell = m_t\bar{n} + \mu_{\ell t}\bar{a}_\ell \end{aligned}$$

and

$$\begin{aligned} &[m_t(\bar{n}\cdot\bar{a}_t)a_t + m_\ell(\bar{n}\cdot\bar{a}_\ell)\bar{a}_\ell]\cdot\nabla r^{-1} \\ &\quad = [m_t\cdot\bar{n} + (m_\ell - m_t)(\bar{n}\cdot\bar{a}_\ell)\bar{a}_\ell]\cdot\nabla r^{-1} \\ &\quad = [m_t\bar{n} + \mu_{\ell t}\bar{a}_\ell]\cdot\nabla r^{-1} \end{aligned} \tag{7}$$

Setting:

$$U_n(\bar{x}) = \frac{1}{4\pi\sigma_0}\int_S m_t\cdot\bar{n}\cdot\nabla r^{-1}\,dS \tag{8}$$

$$U_a(\bar{x}) = \frac{1}{4\pi\sigma_0}\int_S \mu_{\ell t}\bar{a}_\ell\cdot\nabla r^{-1}\,dS \tag{9}$$

we obtain, using Equation 7:

$$\begin{aligned} U(\bar{x}) &= U_n(\bar{x}) + U_a(\bar{x}) \\ &= \frac{1}{4\pi\sigma_0}\int_S [m_t\bar{n} + \mu_{\ell t}\bar{a}_\ell]\cdot\nabla r^{-1}\,dS \end{aligned} \tag{10}$$

In the same way it is also possible to show that $U(\bar{x})$ can be generated by the superposition of the normal and transverse dipole layers $m_\ell\bar{n}$ and $\mu_{t\ell}\,\bar{a}_t$ with $\mu_{t\ell} = (m_t - m_\ell)(\bar{n}\cdot\bar{a}_t)$. The first decomposition seems to be preferable, since the vectors $\bar{n}$, $\bar{a}_\ell$ are directly related to the wavefront and to the fiber direction; the relation is less direct in the case of $\bar{a}_t$.

From Equation 10 some relevant features of the potential field predicted by the model may be easily deduced. Let us assume m_ℓ and m_t constant. Then, if S is a closed surface, as in the case when it is originated by an intramural stimulation, $U_n(\bar{x})$ is zero outside S and only the axial component contributes to the potential field. If S is an open surface, it is well known that $U_n(\bar{x})$, at a distance from S, does not depend on the shape of S but only on its boundary curve (see, e.g., Kellogg, 1953); on the other hand the component $U_a(\bar{x})$ depends both on the shape of S and on the direction of the fibers. $U_a(\bar{x})$ shall give a small contribution whenever the front is almost tangent to the fibers. This condition could be approximately verified in wavefronts of considerable extent, e.g., those in the left ventricular wall when there is a normal sequence of excitation from endocardium to epicardium. In this situation the dominant component in the potential field would be that due to the uniform and normal double layer, thus justifying the use in the QRS complex of this approximate model as an equivalent cardiac generator. On the other hand, if the normal to the front and the local fiber direction are almost parallel, then the axial component is not negligible; it may become dominant with respect to the normal component if the ratio m_ℓ/m_t takes on sufficiently high values. Open wavefronts of this kind can be originated in the ventricular wall after endocardial stimulation.

In the form of Equation 10 and with m_ℓ, m_t constant, the source model we propose may be regarded as an extension of the classical uniform double layer model obtained by the addition of an axial source model. This axial component establishes the dependence of the generated potential field on the shape of the wavefront and on the local fiber orientation with respect to the front. When the axial component becomes negligible the classical model is recovered.

A detailed mathematical treatment of the model described above will be developed elsewhere (Colli et al., 1982). This treatment, based on tensor calculus, will concern the properties of the potential, e.g., the jump relations across the front and the formulation of the problem of the potential in a bounded medium. Therefore, in the following, we shall omit most of the mathematical developments of some complexity and shall state only those results, without proof, which are relevant to support the formulation of the oblique dipole layer model.

Oblique Dipole Layers in a Bounded Isotropic Medium

We shall now consider the potential generated by the axial and transverse dipole layers $\mu_\ell\bar{a}_\ell$, $\mu_t\bar{a}_t$ when the wavefront is imbedded into a homogeneous and isotropic medium which is bounded and insulated.

Let Ω be the bounded region occupied by the medium and Γ its boundary. S denotes, as usual, the wavefront imbedded into the medium; S may be an open or a closed surface. In the last case, let Ω_S be the domain bounded by S. With Ω^* we denote the set of points of Ω which are not in Ω_S or on Γ or on S. The normal to Γ is outward; the normal to S is oriented toward the resting tissue; in particular, if S is closed, the normal to S is outward with respect to Ω_S. Without loss of generality we shall assume that $\sigma_0 = 1$ since, denoting here with $U(\bar{x}; \sigma_0)$ the potential in a medium with conductivity σ_0, it is: $U(\bar{x}; \sigma_0) = U(\bar{x}; 1)/\sigma_0$. In the following, therefore, $U(\bar{x})$ stands for $U(\bar{x}; 1)$.

The bounded medium is assumed insulated, i.e., on Γ the normal component of the electric field is zero, or equivalently $\partial U/\partial n = 0$ on Γ. We set $v(\bar{y}) = U(\bar{y})$ when $\bar{y}$ is on Γ, i.e., v is the potential value on Γ. It can be shown (see, e.g., Miranda, 1970) that for $\bar{x}$ on Γ the potential v satisfies the integral equation:

$$\frac{1}{2} v(\bar{x}) + \frac{1}{4\pi} \int_\Gamma v\bar{n} \cdot \nabla r^{-1} \, d\gamma - \frac{1}{4\pi} \int_S [m_t \bar{n} + \mu_\ell \bar{a}_\ell] \cdot \nabla r^{-1} \, dS = 0 \tag{11}$$

and that for $\bar{x}$ in Ω^* the potential $U(\bar{x})$ is given by:

$$U(\bar{x}) = -\frac{1}{4\pi} \int_\Gamma v\bar{n} \cdot \nabla r^{-1} \, d\gamma + \frac{1}{4\pi} \int_S [m_t \bar{n} + \mu_{\ell t} \bar{a}_\ell] \cdot \nabla r^{-1} \, dS. \tag{12}$$

Once Equation 11 is solved, $U(\bar{x})$ can be computed by means of Equation 12. In Equation 11 it is assumed that Γ has tangent plane in $\bar{x}$; more generally, instead of the coefficient ½ we have the coefficient $\alpha(\bar{x}) = \omega(\bar{x})/4\pi$ where $\omega(\bar{x})$ is the solid angle under which Γ is seen from $\bar{x}$. Denoting with $U_n(\bar{x})$ and $U_a(\bar{x})$ the potential generated in the bounded and insulated medium by the normal and axial dipole layers $m_t\bar{n}$ and $\mu_{\ell t}\bar{a}_\ell$ on S and with v_n, v_a the corresponding values on Γ, it follows that v_n, v_a and U_n, U_a satisfy equations similar to Equations 11 and 12 where v is substituted with v_n or v_a and U is substituted with U_n or U_a. Under the integral sign $\int_S$ we have only $m_t\bar{n} \cdot \nabla r^{-1}$ or $\mu_{\ell t}\bar{a}_\ell \cdot \nabla r^{-1}$. In the case of m_ℓ, m_t constant, denoting with U_n', U_a' the normal and the axial potentials computed for $m_t = 1$, $\mu_\ell t = \bar{n} \cdot \bar{a}_\ell$, it follows that, for any couple m_t, m_ℓ, it is:

$$U(\bar{x}) = m_t U_n'(\bar{x}) + (m_\ell - m_t) U_a'(\bar{x}). \tag{13}$$

The numerical computations which are described in a subsequent section, have been carried out with constant values for the parameters m_ℓ and m_t. As outlined in the Appendix, the model defined by Equation 3 might have also been derived on the basis of assumptions on cellular currents, thus providing, from the electrophysiological point of view, a more adequate basis for the oblique dipole layer model. In this approach, the model parameters m_ℓ, m_t can be interpreted in terms of electrophysiological quantities, namely, the intracellular conductivities along and across the fibers and the intracellular action potential.

Computation of the Extracellular Potential Field

The numerical simulations were carried out for a bounded medium with the following specifications: the isolated and bounded conductor was of the size and shape of the tank used in the experiments on the isolated hearts, i.e., a cylinder 15 cm high and 23 cm across; the medium, isotropic and homogeneous, was considered of conductivity $\sigma_0 = 1$ in the basic calculations. In order to simulate the wavefront as an electrical generator, we assumed its shape to be semi-ellipsoidal when the endocardium was paced, and ellipsoidal for midwall stimulation. In fact, the only information we had about the shape and location of the real wavefront was the site (or sites) where the intramural needle crossed the wavefront. This information could be deduced from the potential profiles along the needle at the instants considered for simulation, and from the time of occurrence of the intrinsic deflection in the intramural electrograms. The remaining features of the simulated wavefront were conjectural but rested on the following, physiologically reasonable assumptions:

α) the wavefront was spreading through straight, parallel fibers. We are aware that the real fibers are not straight, since they follow the curvature of the wall; and they are not parallel, since their direction rotates as a function of depth (Streeter et al. (1969)). However, for very small wavefronts, assumption α) seems acceptable, as seems the hypothesis:

β) m_ℓ, m_t constant (Eq. 13). This last hypothesis means that the electrical behavior of the fibers is identical in the small region we consider;

γ) the ratio of longitudinal to transverse conduction velocity was taken to be 2.14 to 1 [0.6 m/sec longitudinal, 0.28 m/sec transverse, as measured by Baruffi et al. (1978) and Roberts et al. (1979); see also Sano et al. (1959), Draper and Mya-Tu (1959), Meyburg et al. (1978), and Clerc (1979)].

Assumptions α), β), and γ) justify our attributing a semi-ellipsoidal or ellipsoidal shape to the wavefront. A further hypothesis was that endocardial stimulation had not involved the Purkinje network. Since this assumption was not supported by any evidence, we added a new simulation where Purkinje involvement was taken into account.

Finally, at this preliminary stage of our work, we neglected the rotation of fibers in our simulation, and assumed the fibers to run horizontally both at the endocardial level and in the middle of the wall. This was clearly an oversimplification, but had the advantage of enabling the salient features of the simulated field to appear clearly in horizontal sections of the cylindrical conducting medium. In the following, we shall call basis of the front the ellipse which is the intersection of the front with the (flat) endocardial surface or with a surface parallel to the endocardium through the stimulated point, according to whether the stimulation is endocardial or intramural.

One of the axes of the basis was chosen parallel to the cylinder and, for this reason, it is called the vertical axis of the basis. The other axis of ellipse is called the horizontal axis. The third axis of the front is perpendicular to the basis. The following front shapes were considered:

a) with rotational symmetry around the horizontal axis, i.e., the front was generated by rotating a half ellipse 180 degrees around the horizontal axis;

b) as in a) but with rotational symmetry around the third axis (Purkinje involvement);

c) also a closed front surface was considered by taking the whole ellipsoidal surface with rotational symmetry around the horizontal axis.

The potential field, generated by an oblique dipole distribution with constant dipole moments m_ℓ, m_t on the front, at a point $\bar{x}$ of an isolated and bounded domain with

conductivity σ_0 is given by

$$U(\bar{x}) = m_t U_n'(\bar{x}) + (m_\ell - m_t)U_a'(\bar{x}) \quad (14)$$

where U_n', U_a' are, respectively, the normal and axial potentials, with unit dipole moment defined in a previous section.

In order to solve numerically these Equations, the surface of the front and the boundary of the medium were discretized by means of a mesh of triangular elements, and the functions involved were approximated with piecewise linear continuous functions. Using the "collocation method" the problem reduces to the solution of a system of linear equations (Lynn and Timlake, 1968; Jaswon and Symm, 1977).

In all the numerical simulations, the mesh on the front surface included 145 nodes and 264 triangular elements when the front was an open surface of type a) or b); 266 nodes and 528 elements when the front was a closed surface of type c). The mesh of the cylindrical tank surface included 254 nodes and 504 elements.

The two components U_n' and U_a' were calculated at 96 points, evenly distributed on an horizontal section of the tank set at the height of the intramural needle.

The set of these 96 points did not cover the entire section but left out a circular or elongated area around the wavefront. In Figures 8-12, this area, where no equipotential lines are drawn, does *not* correspond to a horizontal section of the heart. The potential at any point of the section was computed by the expression:

$$U = c_1(U_n' + (m_\ell/m_t - 1)U_a') + c_2 \quad (15)$$

where c_1 accounted for the resistivity of the medium and c_2 adjusted the reference value. So that we might compare the simulated potential values to those measured in the isolated dog heart experiments reported here, once the ratio of the parameters m_ℓ/m_t was fixed, we computed the two constants c_1 and c_2 by setting U equal to the potential values measured at two distinct points on the horizontal section. When the purpose of the calculation was to simulate the potential field on the section, without reference to the measured data, then U was computed in arbitrary units by the expression:

$$U = m_t U_n' + (m_\ell - m_t)U_a' \quad (16)$$

Results

Isolated Hearts

The potential distribution in the conducting medium was measured every millisecond. Five milliseconds after the stimulus, the signal-to-noise ratio in the non-averaged electrograms was high enough to enable reliable measurements to be made, at least in the proximity of the heart. By averaging 64 beats on line, the improved signal-to-noise ratio made it possible to obtain acceptable measurements in the whole conducting medium.

Endocardial Pacing

A few milliseconds after delivering the endocardial stimulus, a potential jump amounting to 35 mV or more was observed along the needle at about 1 mm of the stimulating terminal. This jump revealed the intersection of the advancing wavefront with the needle and, between 5 and 8 msec after the stimulus, moved from about 1.5 to 2.5 mm away from the stimulating electrodes. These findings are in agreement with conducting velocities reported in the literature, i.e., 0.22-0.3 m/sec across fibers. The potential distribution along the needle indicated that the current flow was directed toward the wavefront (Fig. 2A).

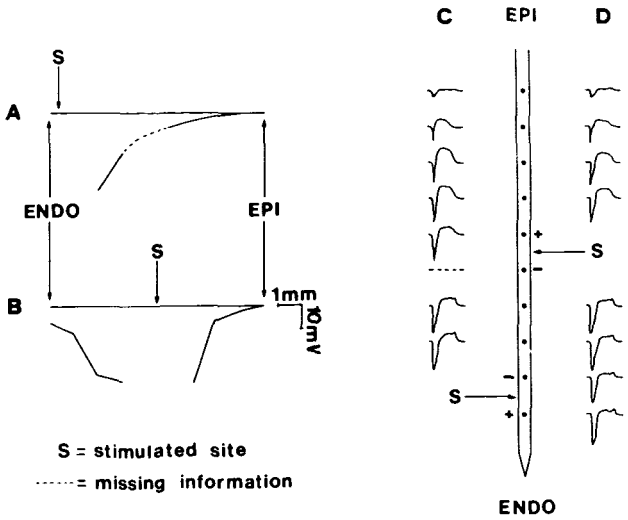

FIGURE 2. *The two profiles are straight plots of the potential recorded by the terminals of the intramural needle 8 msec after endocardial (A) and midwall (B) stimulation. The corresponding electrograms are illustrated in C and D, respectively.*

The potential values recorded by all the terminals located at the tips of the rods enabled us to define the potential distribution on an ideal, open surface surrounding the left half of the heart at a distance of about 5 mm (Fig. 3A). Additional surfaces were gen-

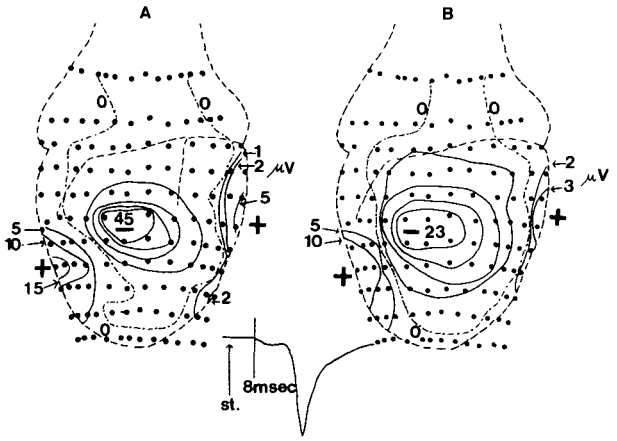

FIGURE 3. *A: Potential distribution on an ideal surface surrounding the left ventricular epicardium at a distance of about 5 mm, at the time instant indicated by the vertical line intersecting the electrocardiogram at the lower end of the figure. This picture was obtained by projecting the tips of the rods supporting the electrodes on a vertical plane perpendicular to the intramural needle. The "minus" sign under the figure "45" (meaning −45 μV) faces the epicardial point where the intramural needle was inserted perpendicularly to the ventricular surface. The pacing stimuli were delivered through the intramural needle, at a sub-endocardial level. B: Same experiment as in A. Potential distribution on a surface surrounding the heart at a distance of about 10 mm at the same time instant. The potential minimum has a lower absolute value as compared to A, indicating that the current flow was directed toward the heart.*

erated by using potential values recorded at increasing distances of the heart (Fig. 3B).

The potential distributions on these surfaces exhibited one minimum and two maxima. The minimum was in the proximity of the axis of the needle, thus facing the advancing wavefront. The maxima were located on the left and right side of the minimum, but the right maximum was generally at a higher vertical level (about 3 cm) compared to the left maximum. Here "left" and "right" are related to the observer, not to the heart. The straight line joining the two maxima in space, when projected on the meridian plane perpendicular to the needle, made an angle of about 30 degrees with the horizontal.

Let us consider an ideal line connecting the points of minimum potential on the sequence of ideal surfaces previously described and surrounding the heart at increasing distance. In our experiments, the potential increased steadily along this line up to the boundary of the tank, thus showing that in a region surrounding the line and reaching the tank wall there was a current flow directed toward the heart. In the same way we can define ideal lines connecting the points of maximum potential. The experimental data enabled us to follow these lines up to a distance of several centimeters of the heart. Moving along these lines, away from the heart, the potential decreased, thus showing the presence of outflowing currents. This behavior of potentials and currents is revealed by the distribution of equipotential lines on a number of horizontal planes in the medium (Fig. 4, A-C). Further evidence is obtained by examining the potential pattern on the wall of the tank (Fig. 5).

Intramural Pacing

After the heart had been paced through two midwall terminals, the wavefront was expected to spread in every direction with a maximum velocity along fibers and a minimum velocity across fibers. The potential profiles along the intramural needle revealed the position of the two intersections between the wavefront and the needle (Fig. 1B). During the time interval considered, between 5 and 8 msec, the wavefront did not reach the endocardium or the epicardium.

The potential values measured along the needle revealed potential gradients and a current flow directed toward those parts of the front that faced the endocardium and the epicardium. In the time interval considered, the potential distribution in the medium showed the same general pattern as observed after endocardial stimulation.

A minimum facing the advancing wavefront and two maxima located on its right and left side were observed on the ideal surfaces surrounding the left ventricular wall (Fig. 6). Since the absolute values of the potentials measured in the tank were lower than those recorded after endocardial stimulation, we could represent the potential distribution only up to a distance of about 2 cm from the epicardium (Fig. 7).

As the positive potentials decreased toward the

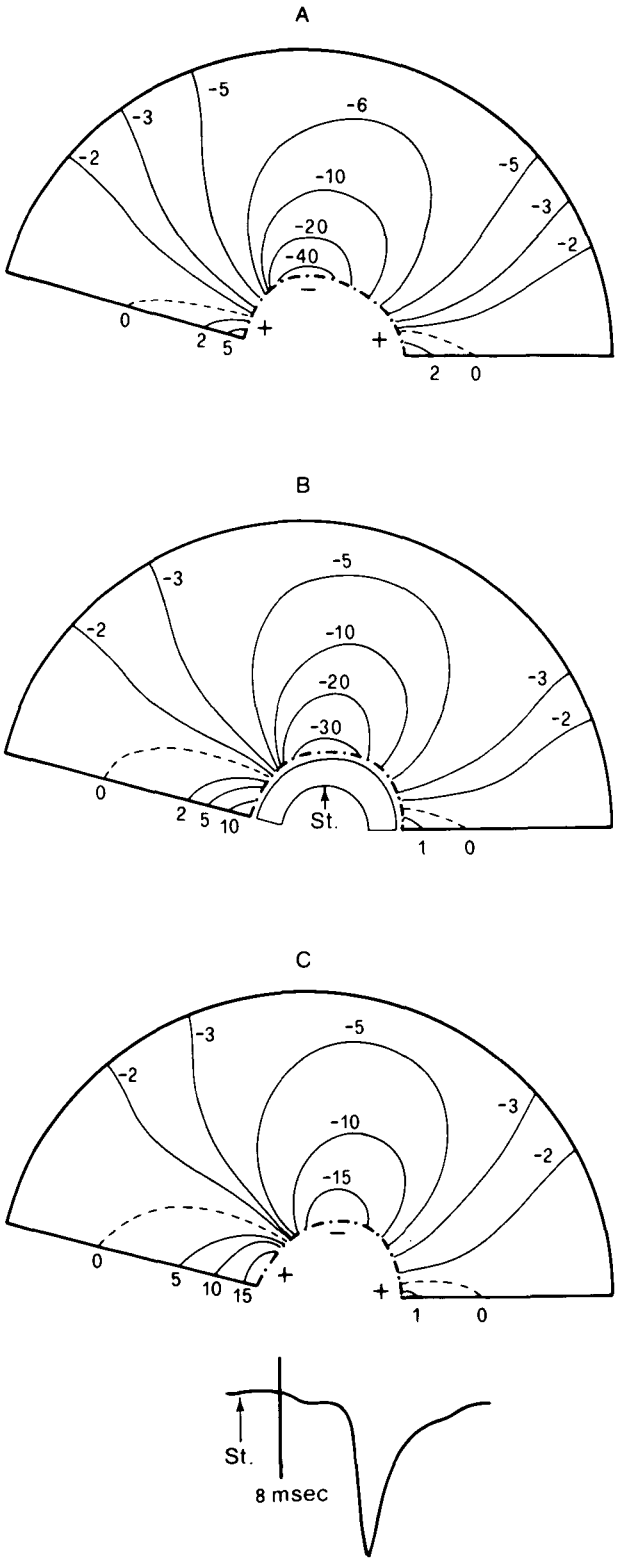

FIGURE 4. *Same experiment as in Figure 3, same time instant. Distribution of equipotential lines in three horizontal planes laying 7 (A), 8 (B), and 9 (C) cm high in the cylinder. The middle plane (B) was approximately at the height of the stimulated point (arrow). The potential gradients show a current flow from the border of the tank toward the heart in those sectors of the medium facing the stimulating electrode. Current is flowing from the heart toward the conducting medium in the two lateral sectors.*

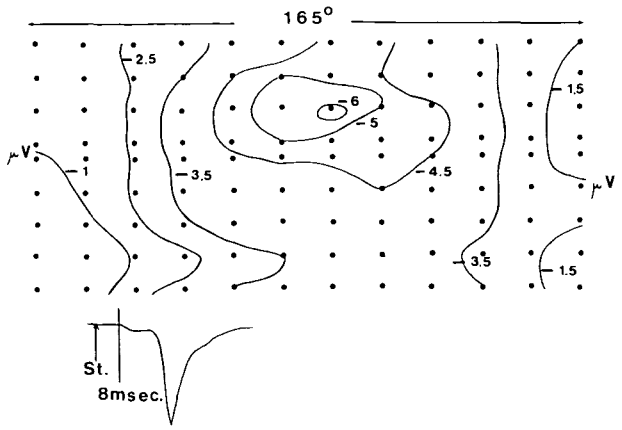

FIGURE 5. *Same experiment as in Figure 3. Potential distribution at the border of the tank. A potential minimum is present in the area facing the stimulating electrode, at a somewhat higher level.*

tank wall and, conversely, the negative potentials increased (smaller absolute values) from the epicardium, a current flow directed toward the central part of the advancing front was present in the conducting medium surrounding the heart.

Some differences could be evidenced in the two experimental conditions. In comparing Figure 2A and Figure 7, it can be observed that the straight lines connecting the two maxima have a different direction. This difference probably is related to the fact that the direction of the fibers in the middle of the wall was rotated in relation to their direction at the subendocardial level (Streeter et al., 1969) (see Discussion).

Moreover, after midwall stimulation, the two maxima lay in two meridian planes which were at an angle

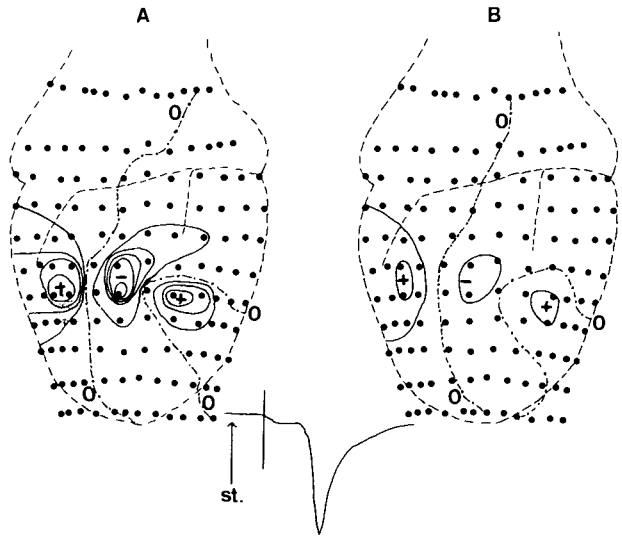

FIGURE 6. *Same heart as in Figure 3. The stimulus was delivered through two terminals at the midwall level. Potential distribution 8 msec after the stimulus, on a surface surrounding the heart at about 5 mm (A) or 10 mm (B) of the epicardium. The potential difference between successive lines is 10 μV. The dashed lines indicate zero potential. The potential pattern is similar to that shown in Figure 3 but the meridian planes containing the two maxima are at a smaller angle between 60 and 75 degrees.*

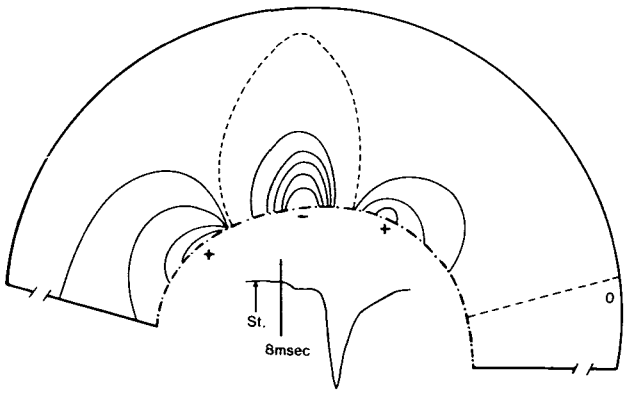

FIGURE 7. *Same experimental conditions as in Figure 6. Potential distribution in a horizontal plane a few millimeters below the level of the stimulating terminals. Two areas are present where the currents flow out of the heart toward the medium. In the region between the two areas, the current flows toward the ventricular surface. The potential difference between successive lines is 10 μV. The dashed lines indicate zero potential. With respect to Figure 4, this picture was magnified about 2 times.*

smaller than that observed after pacing the endocardium.

Model Simulation

The purpose of the model simulations hereafter reported was to verify whether an oblique dipole layer on the wavefront could give rise to potential fields exhibiting the main features of the fields observed in the medium after endocardial and intramural pacing.

Open Wavefront

As stated in "Methods," the simulated wavefront relating to endocardial pacing has the shape of a semi-ellipsoidal surface. The center of the ellipsoid is located at the stimulated point; the major axis lies on the endocardium parallel to the fiber direction which has been supposed to be horizontal; of the two minor axes, one is tangent and the other is perpendicular to the endocardial surface. If the conduction velocity has axial symmetry, then the ellipsoidal surface is axisymmetric in relation to the major axis. At 8 msec after the stimulus, the common length of the minor semiaxes is 2.24 mm and that of the major semiaxis is 4.8 mm. This corresponds to a semi-ellipsoidal wavefront surface of type "a)" (see Methods).

The center of the elliptic front basis was set at the approximate location of the stimulated point, i.e., 8 cm high in the tank and 1.7 cm away from the cylinder axis. Parts A and B of Figure 8 show, respectively, the potential patterns of the components U_n' and U_a', for the described wavefront shape, in a horizontal section 8 cm high in the tank.

Defining the magnitude of each potential distribution as the root mean square (RMS) of the 96 potential values computed on the section, it resulted that the magnitude of the normal component U_n' was about 7 times the magnitude of the axial component U_a'. Therefore, it was expected that in combining linearly

U_n' and U_a' with the dipole moment coefficients m_t and $(m_\ell - m_t)$, respectively, in order to have a non-negligible axial component in the resulting distribution, it should be $m_\ell/m_t > 7$. Superpositions of the two components (Fig. 8, A and B), obtained with ratios m_ℓ/m_t of 10, 15, 20, and 30, are illustrated in Figure 8, C, D, E, and F, respectively.

Note that for $m_\ell/m_t = 10$, a minimum facing the advancing wavefront and two maxima on its left and right side were correctly reproduced. However, the current flow directed toward the advancing front did not extend to the border of the tank but remained a local event. The potential distribution obtained by increasing the ratio m_ℓ/m_t to 20 (Fig. 8E) showed inflowing currents extending in the medium to about half of the tank radius; for this ratio of the parameters the simulated pattern began to match qualitatively the measured one. As the ratio was increased to 30 (Fig. 8F), the area of inflowing currents extended up to the tank border, and for any value of the ratio over 30, the measured pattern could adequately be reproduced with slight differences in the magnitude of the resulting distribution. These results indicated that, in order to reproduce qualitatively the potential pattern measured in the conducting medium 8 msec after endocardial pacing, the axial component should be dominant. The same conclusion was reached in simulating endocardial pacing 5 and 10 msec after the stimulus, always using the conduction velocities $v_t = 0.28$ m/sec and $v_\ell = 0.6$ m/sec to estimate the front surface axes. To investigate how the dominance of the axial component depended on the shape of the wavefront, further simulations were performed with a front in which the major semiaxis was kept at 4.8 mm (i.e., $v_\ell = 0.6$ m/sec) and the minor semiaxes were decreased to 1.6 mm (i.e., $v_t = 0.2$ m/sec). The curvature of the front with respect to the common fiber direction, parallel to the major axis, thus was reduced. With the reduced curvature of the front relative to the fiber direction, the least value of the ratio m_ℓ/m_t which yielded a potential field with features consistent with the measured one, was 35. Conversely, when the front was shaped as a hemisphere of radius 4.8 mm, the magnitude of the normal component U_n' (Fig, 9A) reduced to about 3 times the magnitude of the axial component (Fig. 9B) and the least value of m_ℓ/m_t which yielded a pattern match with the experimental data decreased to 15 (Fig. 9C).

These simulations show that for a given ratio m_ℓ/m_t, the influence of the axial component on the potential field depends on the shape of the front with respect to the fiber orientation. The minimum value of the ratio m_ℓ/m_t which gave rise to a field that matched the real one adequately was between 15 and 30 for the wavefront geometries considered in our simulations.

Closed Wavefront

In simulating the potential field observed 8 msec after intramural pacing, the shape of the wavefront was set as an ellipsoidal surface with axes length and orientation as in the case of the endocardial pacing. The only difference was the location of the center of the ellipsoid, i.e., of the stimulating point, which was deduced from the experimental setup to lay 8 cm high in the tank and 22 mm away from the cylinder axis.

Since in this case the front is a closed surface, the model predicts a normal component U_n' which is constant outside the wavefront. Hence, only the axial component U_a' could be responsible for the variable potential field observed (Fig. 7). This experiment did not allow us to estimate any ratio of the dipole moments. In fact, the simulated potential field on the horizontal section at the level of the stimulating electrode reported in Figure 10, was obtained by fitting the axial component alone to the measured distribution.

In comparing Figure 7 and Figure 10, it may be observed that the two areas where current flew out of the heart toward the medium were correctly reproduced. Moreover, in the simulated distribution, constantly increasing potential values were encountered when moving ahead of the front along a line directed to the tank border. Accordingly, the experimental data showed currents heading toward those parts of the front that moved across fibers. Note that the simulated pattern showed an axial symmetry due to the assumption of parallel fibers and to the symmetry of the front itself. The measured distribution did not show a strictly axial symmetry as observed above. Nevertheless, the simulated pattern presented the same characteristics as the measured one.

Extended Open Wavefront

In order to investigate further how the influence of the axial component depended on the shape of the front, simulations were performed assuming front geometries which could be present in the ventricular wall in the early times of the normal ventricular excitation. Namely, we considered a front shape as might be originated by the endocardial stimulation involving the Purkinje network. If, for sake of simplicity, the Purkinje tissue is assumed to be uniform and continuous, then the intersection of the front with the endocardium, after stimulating one point at the endocardial level, is approximately circular. Since the conduction velocity in the Purkinje tissue is considerably higher than in the working myocardium, the wavefront will have the shape of a convex, almost flat surface (like a watchglass). By taking a Purkinje conduction velocity of 2 m/sec (Scher, 1955), at 8 msec after the stimulus, the radius of the front basis is 16 mm. Following this reasoning, we considered a front shape of type "b)" (see Methods), i.e., a semi-ellipsoidal surface with rotational symmetry with respect to the third axis, which was perpendicular to the endocardium and transverse to the fiber direction. The length of the minor semiaxis was first set to 2.24 mm, i.e., $v_t = 0.28$ m/sec was assumed. Then, in a second simulation, the minor semiaxis was doubled to allow a comparison between the potential fields elicited by the two differently curved wavefronts. The

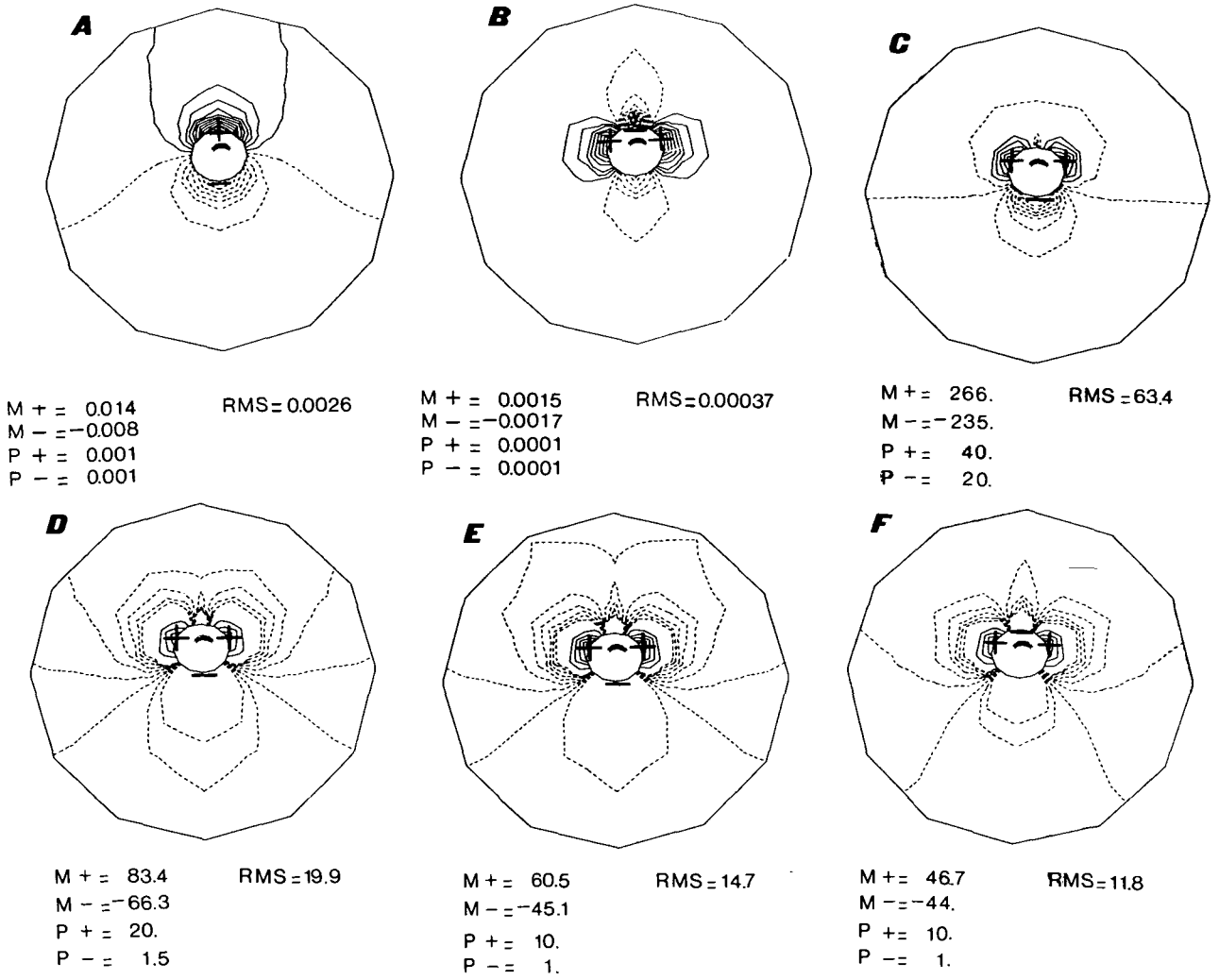

FIGURE 8. *Potential distribution, on a horizontal section of the cylindrical tank at the level of the intramural needle, obtained by stimulating the potential field due to a wavefront spreading in the myocardium 8 msec after endocardial pacing. In each picture, the intersection of the front with the section is represented by the heavy line drawn eccentric with respect to the center of the section. Potential values were computed on eight approximately circular rings, including the outer and the inner ring, 12 values per each ring. The outer ring is an approximation of the tank border and the inner one delimits an area about the front where no potential values were computed. This area does not correspond to the intersection of the heart with the horizontal plane. Equipotential lines were automatically drawn. Solid lines indicate positive potentials; negative and zero potentials are indicated by dashed lines. M+(M−) give the maximum (minimum) value; P+(P−) indicate the step used in drawing positive (negative) equipotential lines. RMS gives the magnitude of the distribution, i.e., the root mean square of the 96 computed potential values. A: Normal component U'_n, i.e., potential field due to a unit and normal dipole layer distributed on the front surface. Potential values are in arbitrary units since, in the basic computations, the conductivity coefficient of the medium was set to unit and the reference value was arbitrary. The typical dipolar pattern is presented with one maximum facing the advancing front and one minimum behind it. Positive potential values progressively decrease and, conversely, negative potential values increase (i.e., become less negative) in moving away from the heart toward the tank wall. B: Axial component U'_a, i.e., potential field due to an axial dipole layer of density given by the cosine of the angle between the unit vector normal to the front and the unit vector along the longitudinal fiber direction (horizontal in the plane of the figure); the two unit vectors point toward the resting tissue. As in A, potential values are in arbitrary units. The negative area in the medium facing the front shows a minimum ahead of the front; two lateral maxima are presented in the longitudinal fiber direction, as expected from the axial dipole distribution. C: Potential distribution obtained by the superposition of U'_n (A) and U'_a (B) with ratio of the dipole moments $m_l/m_t = 10$, then fitted to the measured distribution on the same section (Fig. 4B). The pattern of equipotential line shows that, for this ratio of the parameters, the inflow of currents is limited to a narrow area by the epicardial surface and extends locally in the conducting medium. D, E, F: same as in C with ratios $m_l/m_t = 15, 20, 30$, respectively. While in D the area of inflowing currents ahead of the front is still limited with respect to the measured one, in E the pattern begins to show qualitative agreement with the experimental data. The dominance of the axial component in determining the features of the potential pattern is becoming apparent. However, the area of inflowing current does not extend to the border of the tank. By increasing the ratio m_l/m_t to 30, one obtains pattern F, where the area of inflowing currents extends up to the tank border as in the distribution measured experimentally. Similar patterns are obtained, as expected, when the ratio m_l/m_t is further increased because of the stronger dominance of the axial component. In panels C, D, E, and F, potential values are in μV. To avoid the crowding of lines, only 8 equipotential lines were drawn in the area of negative potentials (dashed lines).*

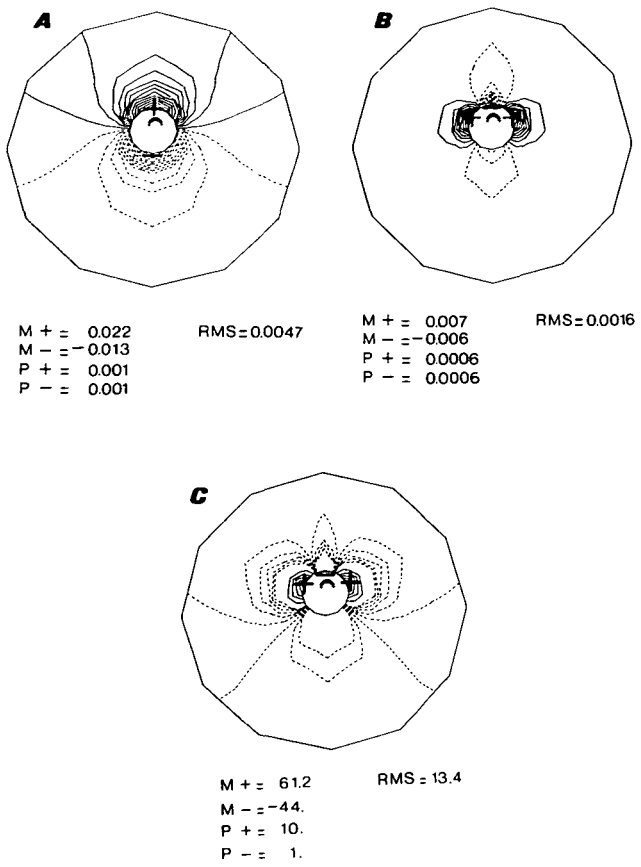

FIGURE 9. *Same as in Figure 8 but relating to a hemispherical wavefront with radius of 4.8 mm. A: Normal component U'_n and B: axial component U'_a, of the potential field in arbitrary units. C: Potential distribution yielded by the superposition of U'_n and U'_a with ratio of the dipole moments $m_\ell/m_t = 15$ and fitted to the measured pattern (Fig. 4B). Compare with Figure 8F, and note that, by varying the shape of the front surface from semi-ellipsoidal to hemispherical, the ratio of the model parameters that yields pattern match with the measured distribution decreases from 30 to 15. Potential values are in μV. As in Figure 8, only eight negative equipotential lines were drawn.*

center of the surface was set, as in the case of endocardial pacing, 8 cm high in the tank and 1.7 cm away from the cylinder axis.

With the first front shape, the magnitude of the normal component U_n' (Fig. 11A) was about 12 times the magnitude of the component U_a' (Fig. 11B). The superposition of these components with the coefficients m_t and $(m_\ell - m_t)$ without fitting to the experimental data are reported in Figure 11, C, D, and E for the parameter ratios m_ℓ/m_t of 5, 10, and 30, respectively. These patterns are reported for comparison with those obtained for the same values of m_ℓ/m_t when the front had the third axis of doubled length. For this front with increased curvature, the magnitude of the normal component U_n' (Fig. 12A) reduced to about 6 times that of the axial component (Fig. 12B). Accordingly, in the patterns obtained by the superposition of the two components (Fig. 12, C, D, E), the appearance of a current flow toward the epicardial areas facing the advancing front and reaching to the tank wall, occurred for a lower value of the ratio m_ℓ/m_t.

To summarize, our results indicated a strong dependence of the magnitude of the axial component on the shape of the wavefront and to the fiber orientation. Approximately, by doubling the front curvature, the magnitude of the axial component was also doubled. Even when the wavefronts were rather flat, like in these last two simulations, potential fields showing the features of those observed after endocardial pacing could be reproduced for values of the model parameters with ratio m_ℓ/m_t in the same range established earlier when fitting the experimental data.

Discussion

Our experiments have been performed with a view to studying the potential distribution in a large conducting medium surrounding an isolated dog heart, after stimulating the left ventricular muscle at the endocardial level or in the middle of the wall. In these experimental conditions, the shape of the wavefront was assumed to be approximately semi-ellipsoidal or ellipsoidal as discussed in the "Methods." Traditionally, the excitation wavefront is considered to be electrically equivalent to a homogeneous distribution of dipoles normally oriented to the surface of the front. By applying this model to a semiellipsoidal wavefront, one would expect the entire surface of the front facing the resting myocardium to generate outflowing currents. In the case of a closed, ellipsoidal surface, no potential gradient would be expected either outside or inside the wavefront.

In recent years a number of studies by other groups and by ourselves have challenged the traditional model. These studies showed that outflowing currents were actually present only on those parts of the front

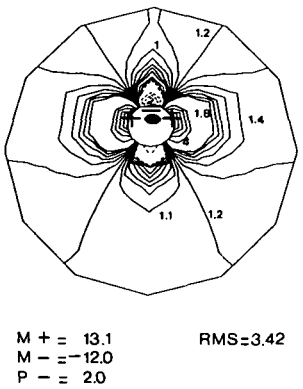

FIGURE 10. *Potential distribution obtained by simulating the potential field due to a closed wavefront surface spreading in the myocardium 8 msec after intramural pacing. Only the axial component U'_a was fitted to the measured distribution (Fig. 7). In this picture, positive equipotential lines were drawn with variable step to give a more detailed description of the low positive potentials in the medium. Namely, from the zeroline, i.e., the outer dashed line, the first 15 positive lines were drawn with a step of 0.1 μV, starting from 0.3 μV, and step of 2 μV was used in the proximity of the two maxima.*

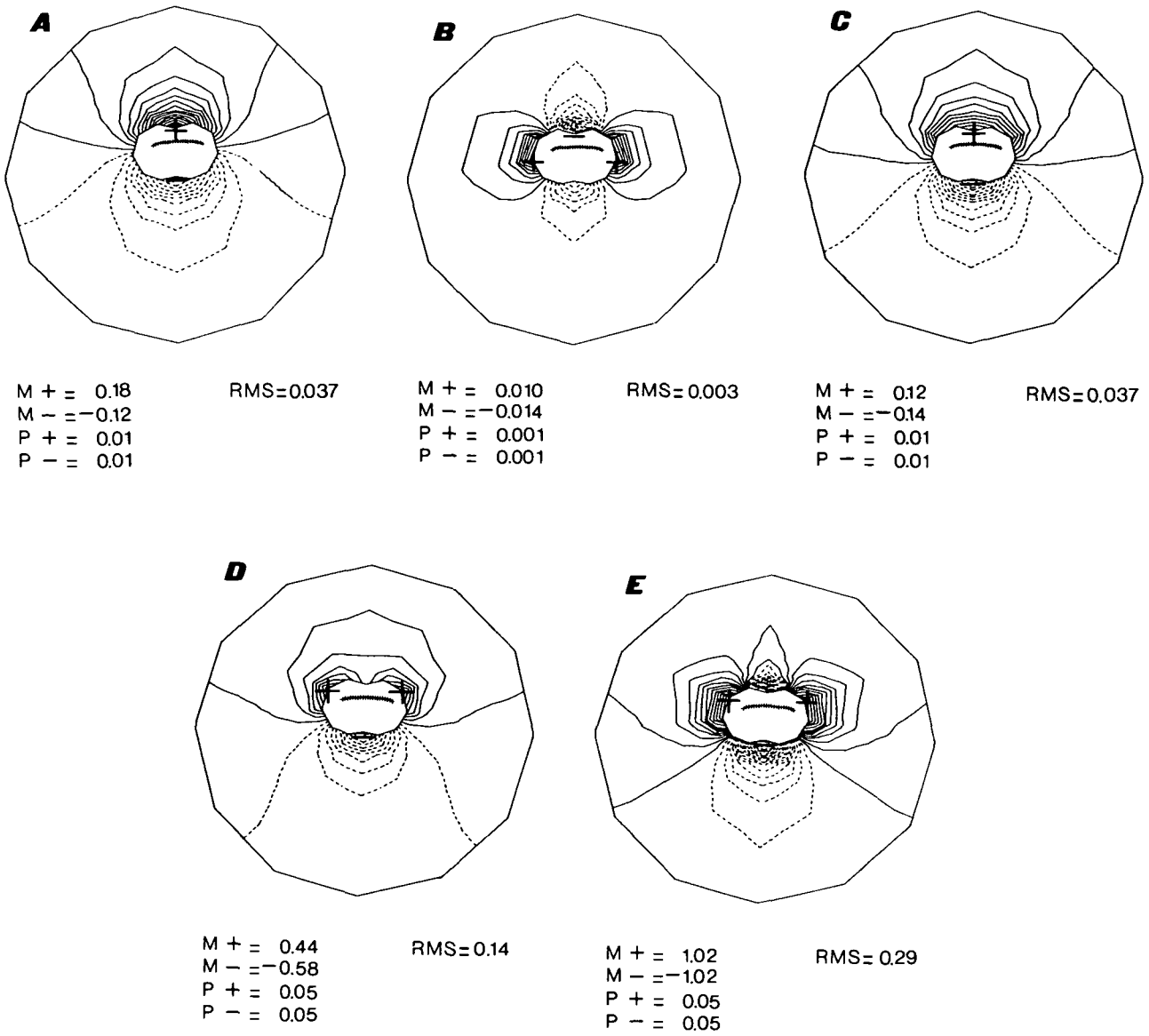

FIGURE 11. *Potential distribution obtained by simulating the potential field due to a semi-ellipsoidal front surface which might originate following endocardial pacing 8 msec after the stimulus, when the Purkinje tissue is involved. A: Normal component U'_n. B: Axial component U'_a of the potential field. C, D, E: Potential distributions obtained by the superposition of U'_n and U'_a with ratios of the dipole moments m_t / m_l = 5, 10, 30, respectively. No fitting to the measured distribution was performed, hence values are in arbitrary units in all the panels. For a ratio of 5, the potential distribution (C) shows the dominance of the normal component; with a ratio of 10 (D), the appearance of the two maxima indicates that the axial components starts to compete with the normal component; last, with a ratio of 30(E), the pattern of equipotential lines clearly indicates the dominance of the axial component (cf. Fig. 8F).*

that moved along the main fiber direction, while a current inflow was present where the front was spreading across fibers. Moreover, sizeable potential gradients were measured outside a closed wavefront obtained by a midwall stimulation (Corbin and Scher, 1977). These findings indicated a strong influence of the fiber orientation on the features of the potential field in the ventricular wall and at the epicardial surface (Corbin and Scher, 1977; Baruffi et al., 1978; Roberts et al., 1979; Roberts and Scher, 1982). Conversely, the investigations mentioned above did not provide any information regarding the features of the potential field at a distance from the heart.

The results of our experiments show that, in the conducting medium surrounding the heart, there was a current flow directed toward the epicardial area overlying the stimulated point. This feature was observed after endocardial and midwall stimulation. Our results cannot be interpreted on the basis of the uniform dipole layer, which in the case of endocardial pacing would generate outflowing currents in all the sectors of the conducting volume facing the advancing wavefront (Wilson et al., 1944), and no current at all after midwall stimulation, as long as the front has not reached the endocardium or the epicardium. Outflowing currents were actually present in the volume on

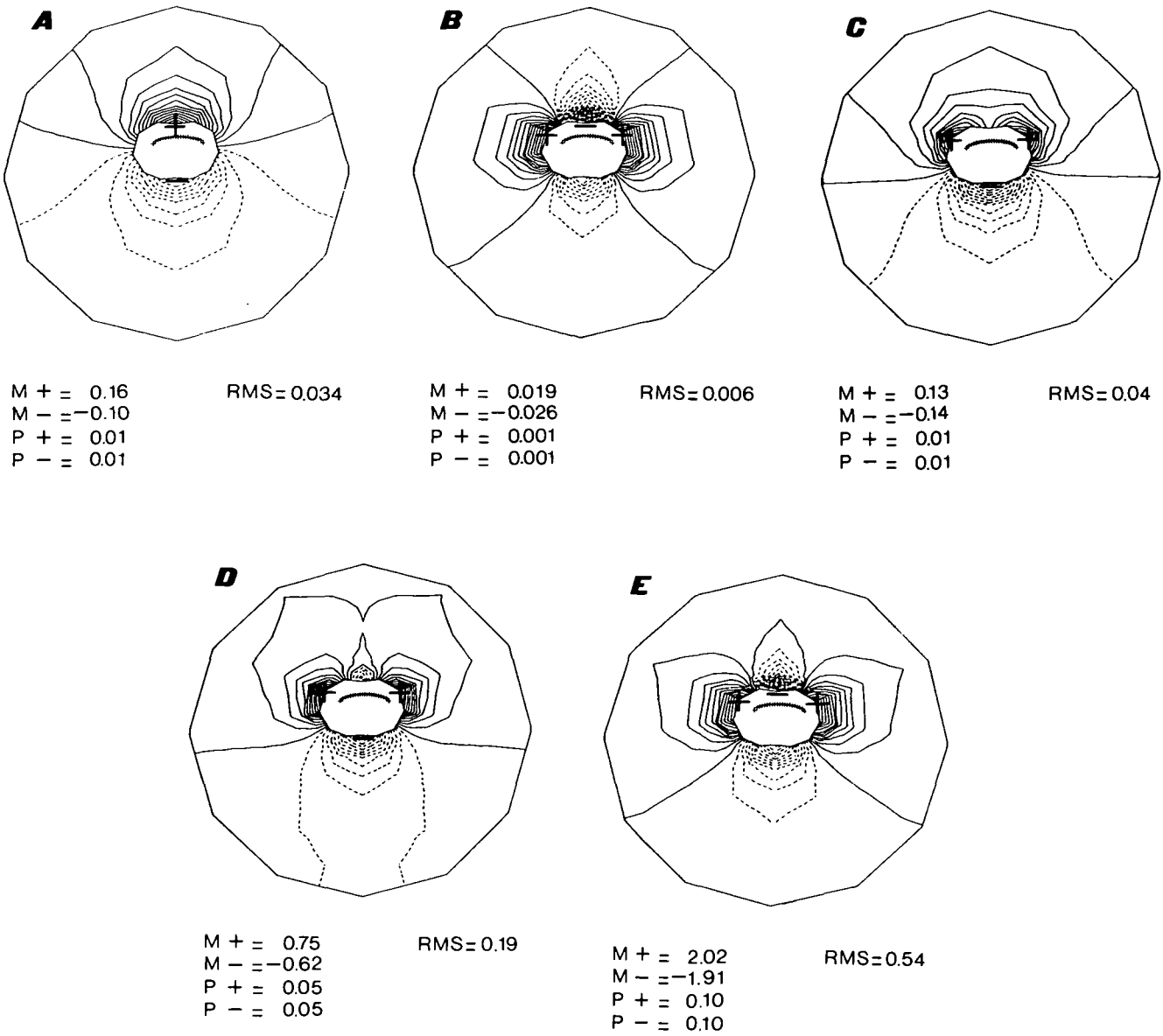

FIGURE 12. *Same as in Figure 11 but relating to a semi-ellipsoidal front surface with the third axis (vertical in the plane of the figure) of doubled length. The potential distribution (C) given by the superposition of the normal (A) and the axial (B) component with a ratio of the dipole moments of 5, is similar to the distribution obtained with a ratio of 10 when the front had reduced curvature (Fig. 11D). Accordingly, in D, where a ratio of 10 is used, the distribution already shows the pattern of inflowing and outflowing currents typical of the case when the axial component is dominant over the normal one.*

the right and left side of the sector where an inflow was observed. This distribution is similar to that observed by Corbin and Scher in the ventricular walls. Our observations, however, extend those presented by the above authors, in that they show that the influence of fiber orientation is still quite sizeable at the border of the tank, at a distance of 10 to 15 times the major axis of the wavefront. Such pattern suggests the presence of a strong axial component in the current generators. If we assume that the main axis of the subendocardial fibers was at +30 ÷ +40 degrees with respect to a horizontal plane, then the presence of two dipoles oriented at 180 degrees along the axis of the fibers would account for a potential and current field similar to the one observed in this study (Fig. 2). Previous experiments with two dipoles oriented at 180 degree along a straight line have shown a similar potential pattern (De Ambroggi and Taccardi, 1970).

Our interpretation is supported by the fact that after midwall stimulation the potential pattern in the medium was similar to that observed after endocardial pacing, but the straight line joining the two epicardial outflow areas was rotated clockwise by approximately 30 to 40 degrees in the various experiments. This is in keeping with the studies of Streeter et al. (1969), showing a clockwise rotation of the fiber axis at different depths in the ventricular wall.

In Streeter's study (1969) for certain locations in

the left ventricular wall, the average rotation was approximately 48 (from +43 to −5) degrees, clockwise when viewed from the outside, with a standard error of 8° and a SD of 18° (see Streeter's Fig. 7B). In our experiments, the average rotation was 35 (from +30 to −5) degrees clockwise, which is qualitatively similar to Streeter's data, except for the lesser degree of rotation. This may be due to the smaller number of experiments we performed or, more likely, to the fact that the directions of the line joining the two extracardiac maxima was not necessarily identical to the fiber directions, although it is certainly related to it. The presence of a very large proportion of horizontal fibers in the ventricular walls (Streeter et al., 1969) brings about a considerable degree of anisotropy of the heart muscle through which the currents spread before leaving the heart. This probably favors the horizontal component of the intracardiac and outflowing currents. In the present stage of our work, the experimental data are still too qualitative to serve as the basis for a realistic, three-dimensional mathematical model. We do not know the exact shape and size of the wavefront, the direction of the fibers through which the front is spreading, or the directions and distribution of the ventricular fibers through which the currents generated by the front actually flow. In addition, we do not know the effect of the interface between heart muscle and extracardiac medium, which is homogeneous, isotropic, and highly conductive, whereas the heart walls are nonhomogeneous, anistropic, and of lower conductivity. Thus, an attempt to perform a refined simulation that would take into account all the above conditions was out of our reach.

On the other hand, a potential distribution similar to the one we observed experimentally could easily be simulated, qualitatively, by an extremely simplified model, i.e., a purely axial model or even two dipoles at 180 degrees, oriented along the hypothetical fiber axis (De Ambroggi and Taccardi, 1970). Such a model, however was not acceptable physiologically, since our knowledge of the equivalent circuits of the heart muscle (including the branching of fibers) implies that there must be a component of the generators oriented across fibers. We added such a component to the axial model and tried to assess which was the maximum strength of the transverse component that would still give a field of the kind we observed at a distance from the sources (we know that, beyond a certain strength, the classical "dipolar" pattern would reappear for a semi-ellipsoidal wavefront). Since we did not know the exact geometry of our wavefronts, we stimulated a number of physiologically plausible wavefront shapes, and we could establish that, for any shape, the transverse component m_t could not be stronger than 1/15 of the axial component m_ℓ, and often had to be as weak as 1/30, in order to generate a realistic potential field. This ratio is not definitive, since our simulation does not take into account the anisotropy of the cardiac volume etc., but nevertheless is probably a fair approximation of the real ratio. Another assumption we had to make was that the ratio m_ℓ/m_t was constant on the whole wavefront surface. By introducing into the model more information (which is obtainable experimentally) on wavefront geometry, fiber direction, etc., we expect to achieve a better definition of m_ℓ/m_t, which should then be applicable to any wavefront of known geometry, provided m_ℓ/m_t is constant and the other characteristics of the system are known.

We also investigated the relationships between our model and the intracellular current model proposed by Spach et al. (1979), in which the jump of the intracellular action potential is assumed to be the same everywhere and the anisotropy of the intracellular conductivity is taken into account. We proved that in the limit case when the intracellular action potential approaches a step function, the model of Spach et al. is equivalent to an oblique dipole distribution which is completely defined by assigning the intracellular axial and transverse conductivity, the constant jump of the intracellular action potential, the fiber direction, and the shape of the front.

A remarkable result which stems from the analysis carried out on our model is that the oblique dipole distribution may also be seen as the superposition of a normal and a purely axial dipole distribution on the front. It is just this axial distribution that introduces the dependence of the potential field on the fiber orientation and the shape of the front. Our model enabled us to reach another interesting conclusion: when the front has the shape of a closed surface, and m_t is constant, only the axial component is effective. This pecularity had not been described in previous papers.

An analysis of the numerical simulations obtained with our model shows a good qualitative agreement with the experimental data. In fact, for suitable values of the model parameters, the number and approximate location of the minima and maxima are correctly reproduced, as well as the overall potential distribution up to the tank wall and the patterns of inflowing and outflowing currents. This agreement between model prediction and experimental data supports the idea that it is possible to represent the equivalent generators by means of a dipole distribution which, however, is not purely normal or axial. In particular, in simulating the experimental data here reported, we found that the axial component of the potential field played a dominant role with respect to the normal component.

In conclusion, an oblique dipole layer source model proved adequate to predict a set of potential fields generated by paced dog hearts in a volume conductor.

On the basis of these results, we believe that an oblique dipole layer source model could be suited to predict the potential fields related to realistic wavefronts as those spreading through the myocardium during a normal sequence of excitation in the ventricular walls. However, we do not believe that the dominance of the axial component, which was evidenced by our data, would hold true under any circumstance.

Our model actually predicts that the influence of the axial component will decrease as the front surface tends to become parallel to the fiber direction, a condition that is likely to occur during part of the normal depolarization process.

Having in mind the solution of the forward problem, that is, the prediction of body surface maps from the distribution of the active areas in the heart, we feel it is important to establish the contribution of the normal and axial component over the whole front.

Appendix

The equivalent source generators of the heart are related to the electrophysiological activity of the heart and must therefore be explained on such a basis. An analysis of different formulations of the potential field generated by a single active fiber in a volume conductor has been carried out by Plonsey (1974). Miller and Geselowitz (1978), Spach et al. (1979), and Plonsey and Rudy (1980) have developed models concerning the potential generated by a continuum of fibers.

Oblique Dipole Layers and Anisotropic Intracellular Conductivity

In formulating the oblique double layer model represented by Equation 3, no particular assumptions were made about the coefficients m_ℓ, m_t. We shall now try to correlate these coefficients to some definite electrophysiological quantities, namely, to the intracellular conductivity along and across the fiber and to the intracellular action potential jump. This relation is established under the assumption of an instantaneous depolarization process. We shall in particular show how a limit case of Spach's et al. (1979) intracellular current model is related to our model. In their model, the heart tissue is conceived as the superposition of the anisotropic intracellular (i) medium and the isotropic extracellular (e) medium. The following assumptions are made: (1) the (e) medium is homogeneous and isotropic with conductivity σ_0; (2) the fibers are parallel and axisymmetric with respect to the intracellular conductivity; and (3) the (i) medium is characterized by the axial and transverse conductivity coefficients σ_ℓ^i, σ_t^i.

We can utilize cartesian coordinates in which one of the axes (say the third) is parallel to the common fiber direction; in this coordinate system the intracellular conductivity is characterized by the three coefficients $\sigma_1^i = \sigma_2^i = \sigma_t^i$ and $\sigma_3^i = \sigma_\ell^i$. Moreover, we denote with U_i and U_e the intracellular and the extracellular potential. From the current conservation law, and setting $U = U_e$, it follows that:

$$\sigma_0 \Delta U = I_m = \frac{\partial}{\partial x_1}\left(\sigma_1 \frac{\partial U_i}{\partial x_1}\right) + \frac{\partial}{\partial x_2}\left(\sigma_2 \frac{\partial U_i}{\partial x_2}\right) + \frac{\partial}{\partial x_3}\left(\sigma_3 \frac{\partial U_i}{\partial x_3}\right)$$

where I_m is the transmembrane current per unit volume of tissue and $\Delta = \nabla \cdot \nabla$. Therefore the potential U is given by (see Plonsey, 1969):

$$U(\bar{x}) = \frac{1}{4\pi\sigma_0} \int_{V_a} r^{-1} I_m \, dV. \qquad (17)$$

The volume V_a is the "activating" region i.e. the seat of intracellular currents. This region is bounded by two surfaces, S_r and S_a. On S_r, the depolarization process has just started; on S_a, it has just been completed; in between, the process is under way. If the normal to S_r and S_a is oriented toward the resting tissue, then ahead of S_r there is resting tissue, whereas behind S_a there is depolarized tissue; $I_m \neq 0$ only in V_a.

It also is assumed that all cardiac cells undergo the same depolarization process, i.e., the temporal shape of the intracellular action potential is common to all cells with a monotone variation from the resting value u_r to the plateau value u_a. From these assumptions, it can be shown that:

$$\int_{V_a} r^{-1}\left(\frac{\partial}{\partial x_1}\left(\sigma_1 \frac{\partial U_i}{\partial x_1}\right) + \frac{\partial}{\partial x_2}\left(\sigma_2 \frac{\partial U_i}{\partial x_2}\right) + \frac{\partial}{\partial x_3}\left(\sigma_3 \frac{\partial U_i}{\partial x_3}\right)\right) dV$$

$$= -\int_{V_a}\left(\sigma_1 \frac{\partial U_i}{\partial x_1}\frac{\partial r^{-1}}{\partial x_1} + \sigma_2 \frac{\partial U_i}{\partial x_2}\frac{\partial r^{-1}}{\partial x_2} + \sigma_3 \frac{\partial U_i}{\partial x_3}\frac{\partial r^{-1}}{\partial x_3}\right) dV \qquad (18)$$

Therefore:

$$U(\bar{x}) = -\frac{1}{4\pi\sigma_0}\int_{V_a}\left(\sigma_1 \frac{\partial U_i}{\partial x_1}\frac{\partial r^{-1}}{\partial x_1} + \sigma_2 \frac{\partial U_i}{\partial x_2}\frac{\partial r^{-1}}{\partial x_2} + \sigma_3 \frac{\partial U_i}{\partial x_3}\frac{\partial r^{-1}}{\partial x_3}\right) dV \qquad (19)$$

In Equation 18 the active sources are not restricted to the wavefront surface as in Equations 1 and 3. Therefore the model of Spach et al. may be more suitable for studying the potential in proximity of the sources, e.g., in the myocardium. If the depolarization process is very short, V_a is very thin and S_r, S_a tend to coincide with the wavefront surface S. In the limit, for an instantaneous depolarization process with an intracellular action potential jump from u_r to u_a across S, it may be shown that Equation 19 tends to:

$$U(\bar{x}) = \frac{u_a - u_r}{4\pi\sigma_0}\int_S (\sigma_t^i(\bar{n}\cdot\bar{a}_t)\bar{a}_t + \sigma_\ell^i(\bar{n}\cdot\bar{a}_\ell)\bar{a}_\ell)\cdot\nabla r^{-1}\, dS \qquad (20)$$

It follows immediately that Equation 20 can be deduced from Equation 3 by setting:

$$m_t = (u_a - u_r)\sigma_t^i \qquad m_\ell = (u_a - u_r)\sigma_\ell^i \qquad (21)$$

We have also:

$$m_\ell / m_t = \sigma_\ell^i / \sigma_t^i.$$

The whole development concerning Equations 17, 19, and 20 may be carried out under the more general assumption of variable fiber direction. This is done in the previously mentioned paper about the mathematical analysis of the oblique dipole layers.

Oblique Dipole Layers in a Uniform, Anisotropic Medium

We shall now consider extensions of the model given by Equation 3 to the case of an unbounded anisotropic extracellular medium. These models should be more adequate to describe the local potential field in the myocardial tissue near the excitation wavefront. To this end, we drop the assumption that the extracellular medium has isotropic constant conductivity σ_0. The myocardial tissue is assumed to be represented by two parallel uniform and anistropic media: the intracellular (i) and the extracellular (e) media. Axial symmetry of the fiber properties is still assumed. In a system of cartesian coordinates with the third axis parallel

to the common fiber direction, let $\sigma_1^e = \sigma_2^e = \sigma_t^e$ and $\sigma_3^e = \sigma_\ell^e$ be the conductivity coefficients in (e); the corresponding coefficients in (i) have already been introduced. The uniformity of the two media implies that all conductivity coefficients are constant. To state that all cells act identically from the electrophysiological point of view, two different hypotheses may be assumed: Either the intracellular action potential (IAP) or the transmembrane action potential (TAP) has the same temporal shape for all cells. Depending on whether we assume IAP or TAP, starting from the continuity of current in the myocardium, two models are derived for the extracellular potential when the shape of the IAP or of the TAP approaches a step function. These two models show the same mathematical structure; the expression for the potential $U(\bar{x})$ may be formally derived from Equation 20 in the following way. Setting $\alpha = u_a - u_r$ and $\phi = \sigma_0 r$, formula 20 becomes:

$$U(\bar{x}) = \frac{\alpha}{4\pi}\int_S (\sigma_t^i(\bar{n}\cdot\bar{a}_t)\bar{a}_t + \sigma_\ell^i(\bar{n}\cdot\bar{a}_\ell)\bar{a}_\ell)\cdot\nabla\phi^{-1}\,dS \quad (22)$$

$\phi^{-1} = (\sigma_0 r)^{-1}$ can be interpreted as the potential generated at $\bar{x}$ by a unit charge placed at $\bar{y}$ in a homogeneous isotropic medium. In the case of IAP, we keep $\alpha = u_a - u_r$; in the case of TAP, we set $\alpha = \psi_a - \psi_r$ where ψ_a, ψ_r are the plateau and the resting values of the transmembrane potential. ϕ^{-1} must represent the potential value at $\bar{x}$ due to a unit charge at $\bar{y}$ placed in a uniform anisotropic medium with conductivity coefficients along the coordinate axes given by:

$$\begin{cases} \sigma_k = \sigma_k^e & k = 1, 2, 3 \quad \text{for (IAP)} \\ \sigma_k = \sigma_k^i + \sigma_k^e & k = 1, 2, 3 \quad \text{for (TAP)} \end{cases} \quad (23)$$

In the last case, σ_1, σ_2, σ_3 may be interpreted as the conductivity coefficients of the anisotropic myocardial tissue. ϕ is given by:

$$\phi(\bar{x}, \bar{y}) = (\sigma_2\sigma_3(x_1 - y_1)^2 + \sigma_3\sigma_1(x_2 - y_2)^2 + \sigma_1\sigma_2(x_3 - y_3)^2)^{1/2} \quad (24)$$

If $\sigma_1 = \sigma_2 = \sigma_3 = \sigma_0$, we get $\phi = \sigma_0 r$. Furthermore, we remark that the potential defined by Equation 22 is the superposition of the potentials generated by an axial and a transverse dipole layer of density $\sigma_\ell^i(\bar{n}\cdot\bar{a}_\ell)$ and $\sigma_t^i(\bar{n}\cdot\bar{a}_t)\bar{a}_t$ in the anisotropic medium (e). Hence the dipolar moments m_ℓ and m_t are still given by relations similar to those derived in the case of the isotropic extracellular medium i.e. $m_\ell = \alpha\sigma_\ell^i$, $m_t = \alpha\sigma_t^i$.

It can easily be proved that:

$$\sigma_t^i(\bar{n}\cdot\bar{a}_t)\bar{a}_t + \sigma_\ell^i(\bar{n}\cdot\bar{a}_\ell)\bar{a}_\ell = \frac{\sigma_t^i}{\sigma_t}\bar{\nu} + \left(\sigma_\ell^i - \frac{\sigma_t^i\sigma_\ell}{\sigma_t}\right)(\bar{n}\cdot\bar{a}_\ell)\bar{a}_\ell$$

where:

$$\bar{\nu} = \sigma_t(\bar{n}\cdot\bar{a}_t)\bar{a}_t + \sigma_\ell(\bar{n}\cdot\bar{a}_\ell)\bar{a}_\ell$$

Then we obtain the following splitting which generalizes Equation 10 given in "Methods" to an anisotropic medium:

$$U(\bar{x}) = \frac{\alpha}{4\pi}\left\{\frac{\sigma_t^i}{\sigma_t}\int_S \bar{\nu}\cdot\nabla\phi^{-1}\,dS + \left(\sigma_\ell^i - \frac{\sigma_t^i\sigma_\ell}{\sigma_t}\right)\int_S (\bar{n}\cdot\bar{a}_\ell)\bar{a}_\ell\cdot\nabla\phi^{-1}\,dS\right\} \quad (25)$$

Using the notation of conormal direction associated to an elliptic operator, it can be proved (see Miranda, 1970, ch. II, § 5, pp. 39-43) that for a closed surface S and $\bar{x}$ exterior to S it results:

$$\int_S \bar{\nu}\cdot\nabla\phi^{-1}\,dS = 0$$

Therefore in the case of a closed surface, the *potential depends only on the axial component*, in both an isotropic and an anistropic medium.

Drs. Colli-Franzone, Guerri, and Viganotti are affiliated with the Institute of Numerical Analysis, Dr. Macchi with the Institute of the Application of Calculus, and Drs. Baruffi, Spaggiari, and Taccardi with the Institute of General Physiology.

Address for reprints: Piero Colli-Franzone, Istituto di Analisi Numerica del C.N.R. C.so C. Alberto, 5, 27100 Pavia, Italy.

Received July 7, 1981; accepted for publication June 4, 1982.

References

Baruffi S, Spaggiari S, Stilli D, Musso E, Taccardi B (1978) The importance of fiber orientation in determining the features of cardiac electric field. *In* Modern Electrocardiology, edited by Z Antaloczy. Amsterdam, Excerpta Medica, pp 89-92

Clerc L (1976) Directional differences of impulse spread in trabecular muscle from mammalian heart. J Physiol (Lond) **255:** 335-345

Colli Franzone P, Guerri L, Viganotti C (in press) Oblique dipole layers applied to electrocardiology. J Math Biol

Corbin LV II, Scher AM (1977) The canine heart as an electrocardiographic generator: Dependence on cardiac cell orientation. Circ Res **41:** 58-67

Cottini C, Dotti D, Gatti E, Taccardi B (1976) A 240-probe instrument for mapping cardiac potentials. *In* Proceedings of the Satellite Symposium of the XXV International Congress of Physiological Sciences: The electrical field of the heart, edited by P Rijlant. Bruxelles, Presses Académiques Européennes, pp 99-102

De Ambroggi L, Taccardi B (1970) Current and potential fields generated by two dipoles. Circ Res **27:** 901

Draper MH, Mya-Tu M (1959) A comparison of the conduction velocity in cardiac tissue of various mammals. Q J Exp Phys **44:** 91-109

Jaswon MA, Symm GT (1977) Integral equation methods in potential theory and elastostatics, London, Academic Press

Kellogg OD (1953) Foundations of Potential Theory. New York, Dover Publications

Lynn MS, Timlake WP (1968) On the numerical solution of the singular integral equation of potential theory. Numer Math **11:** 77-98

Miller WT III, Geselowitz DB (1978) Simulation studies of the electrocardiogram. I. The normal heart. Circ Res **43:** 301-315

Miranda C (1970) Partial Differential Equations of Elliptic Type. Berlin Heidelberg, Springer-Verlag

Myerburg RJ, Gelband H, Nilsson K, Castellanos A, Mirales AR, Basset AL (1978) The role of canine superficial ventricular muscle fibers in endocardial impulse distribution. Circ Res **42:** 27-35

Plonsey R, Fleming D (1969) Bioelectric Phenomena. New York, McGraw-Hill, pp 202-275

Plonsey R (1974) The active fiber in a volume conductor. IEEE Trans BME 21, **5:** 371-381

Plonsey R, Rudy Y (1980) Electrocardiogram sources in a 2-dimensional anisotropic activation model. Med Biol Eng Comput **18:** 87-94

Roberts DE, Scher AM (1982) Effect of tissue anisotropy on extracellular potential fields in canine myocardium in situ. Circ Res **50:** 342-351

Roberts DE, Hersh LT, Scher AM (1979) Influence of cardiac fiber

orientation on wavefront voltage, conduction velocity and tissue resistivity in the dog. Circ Res **44:** 701-712

Sano T, Takayama N, Shimamoto T (1959) Directional difference of conduction velocity in the cardiac ventricular syncytium studied by microelectrodes. Circ Res **7:** 262-267

Scher AM (1955) Direct recording from the A. V. conducting system in the dog and monkey. Science **121:** 398

Spach MS, Barr RC, Serwer GA, Kootsey JM, Johnson EA (1972) Extracellular potentials related to intracellular action potentials in the dog Purkinje system. Circ Res **30:** 505-519

Spach MS, Miller WT, Miller-Jones E, Warren RB, Barr RC (1979) Extracellular potentials related to intracellular action potentials during impulse conduction in anisotropic canine cardiac muscle. Circ Res **45:** 188-204

Spaggiari S, Baruffi S, Macchi E, Arisi F, Stilli D, Musso E, van Dam RT, Taccardi B (1982) Is the uniform dipole layer an adequate model of the excitation wavefront? *In* Proceeding of the 7th International Congress on Electrocardiology: New Frontiers in Electrocardiology, edited by F de Padua and PW Macfarlane. Chichester, Wiley

Streeter DD Jr, Spotnite MM, Patel DP, Ross J Jr, Sonnenblick EH (1969) Fiber orientation in the canine left ventricle during diastole and systole. Circ Res **24:** 339-347

Taccardi B, Musso E, De Ambroggi L (1972) Current and potential distribution around an isolated dog heart. *In* Proceedings of the Satellite Symposium of the XXV International Congress of Physiological Sciences: The Electrical Field of the Heart, edited by P Rijlant. Bruxelles, Presses Académiques Européennes, pp 566-572

Wilson FN, Johnston FD, Rosenbaum FF, Erlanger H, Kossmann CE, Hecht H, Cotrin N, Menezes de Oliveira R, Scarfi R, Barker PS (1944) The precordial electrocardiogram. Am Heart J **27:** 19-85

INDEX TERMS: Electrocardiology · Cardiac electric field · Myocardial anisotropy · Forward problem